Material deformation in a restricted Euler model for turbulent flows: Analytic solution and numerical tests

Yi Li and Charles Meneveau
Department of Mechanical Engineering and Center for Environmental and Applied Fluid Mechanics, The Johns Hopkins University, Baltimore, Maryland 21218

(Received 22 May 2006; accepted 7 December 2006; published online 25 January 2007)

The restricted Euler (RE) approximation applied to the equation of the velocity gradient tensor has been shown [Cantwell, Phys. Fluids A **4**, 782 (1992)] to reproduce important geometric trends concerning small scale structures in Navier-Stokes turbulence. In this paper, the Lagrangian evolution of material volume elements as they are deformed in a turbulent flow is considered. First, it is shown that the equation for the deformation tensor evolving under RE dynamics admits an analytic solution similar to that of the velocity gradient tensor. The evolution of the eigenvalues and eigenvectors of the Cauchy-Green tensor is obtained from this analytic solution. Comparison with direct numerical simulations (DNS) is performed. Results show that the analytic prediction of shapes and orientations of fluid volume elements agrees well with DNS for an evolution time scale of the order of the Kolmogorov time scale, which is also the time it takes for significant material element deformation. The analysis is repeated in the inertial range, where the deformation due to a filtered velocity field is considered. The analytic solution with filtered velocity gradients as initial conditions is evaluated. Good agreement is found for longer (turn-over) durations, of the order of the eddy turn-over time at the filter scale. © *2007 American Institute of Physics*.
[DOI: 10.1063/1.2432913]

I. INTRODUCTION

The Lagrangian evolution of the small scale geometry of turbulent flow has received considerable attention since the works of Vieillefosse[1] and Cantwell[2] on the restricted Euler (RE) dynamics for velocity gradients.[3–8] In RE dynamics, the viscous diffusion term is neglected, and the pressure Hessian is assumed to be isotropic, leading to a closed ordinary differential equation for the velocity gradient tensor. Vieillefosse[1] and Cantwell[2] showed that the equation admits an analytic solution for the Lagrangian evolution of the velocity gradient. The solution shows that RE dynamics captures many important trends observed in direct numerical simulations (DNS) and experiments,[9–11] including the preferential alignment of vorticity with the intermediate eigendirection of the strain rate tensor and the prevalence of axisymmetric expanding motions.

RE dynamics is not without its problems, since it predicts unphysical finite-time singularities[2] and displays various differences with true Navier-Stokes (NS) dynamics. Nevertheless, with analytically treatable solutions for the full tensor-level, nonlinear dynamics of fluid turbulence, RE dynamics has provided a fruitful starting point for further progress. For instance, RE dynamics has been the starting point of several models of the velocity gradient tensor.[12–15] One idea is to make use of the evolution of material deformation to regularize the finite time singularity in RE dynamics, and to make connection with the length scale associated with the velocity gradient tensor. In prior work, the information of material deformation is obtained by following either the evolution of tetrads[13,15] or the Cauchy-Green (CG) tensor.[14] Recently, a stochastic model for the velocity gradient tensor that incorporates a simplified closure based on material deformation has been proposed.[16]

Motivated by the above developments, we now consider the evolution of material deformation when the velocity gradient tensor evolves according to the RE dynamics. Material deformation will be characterized by the deformation and the Cauchy-Green tensors.[17,18] Suppose $\mathbf{x}=\mathbf{x}(\mathbf{X},t)$ is the position of a fluid particle at time t whose initial reference position was $\mathbf{X}$. At time t, the component B_{ij} of the deformation tensor $\mathbf{B}(\mathbf{X},t)$ for fluid particle $\mathbf{X}$ is defined as $B_{ij}=\partial x_j(\mathbf{X},t)/\partial X_i$.[17] As sketched in Fig. 1, an arbitrary infinitesimal material line $\delta\mathbf{X}$ attached to $\mathbf{X}$ will be advected, rotated, and stretched in a flow field, and, at a later time t, becomes $\delta\mathbf{x}(\mathbf{X},t)$ and locates at $\mathbf{x}$. From the definition of $\mathbf{B}$, it is evident that $\delta\mathbf{x}$ is given by $\delta\mathbf{x}=\delta\mathbf{X}\mathbf{B}$.[17] Therefore, $\mathbf{B}$ represents the cumulative effects of stretching and rotation of an infinitesimal material line along its trajectory, and determines its length and orientation in its evolution. The corresponding CG tensor is defined as $\mathbf{C}(\mathbf{X},t)=\mathbf{B}^{\mathrm{T}}\mathbf{B}$. It is easy to establish that $|\delta\mathbf{X}|^2=\delta\mathbf{x}\mathbf{C}^{-1}\delta\mathbf{x}^{\mathrm{T}}$, which, for constant $|\delta\mathbf{X}|$, represents an ellipsoid characterized by $\mathbf{C}$. A spherical material volume with radius $|\delta\mathbf{X}|$ evolves into an ellipsoid, with major axis lengths and orientations given by the square roots of the eigenvalues and by the eigenvectors of $\mathbf{C}$, respectively.[17]

The Lagrangian evolution of material elements has been extensively studied in various works.[18–23] In Sec. II we show that when the velocity gradient tensor is approximated by RE dynamics, an analytic solution can be obtained for the Lagrangian evolution of the deformation tensor $\mathbf{B}$. In Sec.

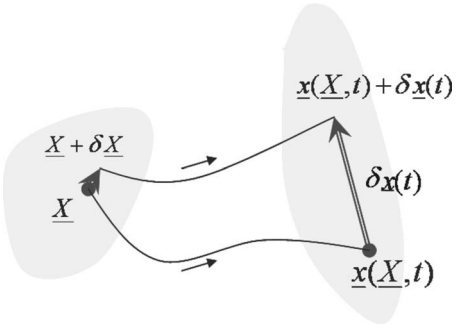

FIG. 1. A sketch of the evolution a small material line element $\delta\mathbf{X}$ in a flow field, which is initially attached to fluid particle $\mathbf{X}$.

III, the solution is compared with DNS data in terms of the eigenvalues and orientation of the CG tensor calculated from the solution. Results are discussed in Sec. IV.

II. ANALYTIC SOLUTION TO THE DEFORMATION TENSOR

We begin by briefly reviewing the analytic solution to the RE approximation to the Navier-Stokes equations. For generality, we write it in the context of the NS equations filtered at some arbitrary scale Δ. The unfiltered case is simply obtained by setting $\Delta=0$ and dropping the additional stresses introduced by the filtering operation. The filtered NS equations read

$$\frac{d\tilde{u}_i}{dt} \equiv \partial_t\tilde{u}_i + \tilde{u}_l\partial_l\tilde{u}_i = -\partial_i\tilde{p} - \partial_j\tau_{ij} + \nu\partial_{kk}^2\tilde{u}_i, \tag{1}$$

where $\tilde{p}$ is pressure divided by density. $\tau_{ij}\equiv\widetilde{u_iu_j}-\tilde{u}_i\tilde{u}_j$ is the subgrid-scale (SGS) stress tensor accounting for scales eliminated by the filtering. In addition, incompressibility implies that $\partial_i\tilde{u}_i=0$. Defining the filtered velocity gradient tensor $\tilde{A}_{ij}=\partial\tilde{u}_j/\partial x_i=\partial_i\tilde{u}_j$, its evolution equation[8,24] is obtained by taking the gradient of Eq. (1):

$$\frac{d\tilde{A}_{ij}}{dt} = -\left[\tilde{A}_{ik}\tilde{A}_{kj} + \frac{2}{3}Q\delta_{ij}\right] + H_{ij}, \tag{2}$$

where $Q=-\tilde{A}_{mn}\tilde{A}_{nm}/2$ is the second invariant of $\tilde{A}_{ij}$, which in incompressible flows also equals the isotropic part of the gradients of the pressure, SGS, and viscous forces. The Hessian tensor H_{ij}, which includes the anisotropic part of the forces, is defined as

$$H_{ij} = -\partial_{ij}^2\tilde{p} - \partial_{ik}^2\tau_{jk} + \tfrac{1}{3}\delta_{ij}(\partial_{kk}^2\tilde{p} + \partial_{km}^2\tau_{km}) + \nu\partial_{kk}^2\tilde{A}_{ij}. \tag{3}$$

The RE equation for $\tilde{A}_{ij}$ is obtained from (2) by neglecting H_{ij} altogether,[1,2] giving

$$\frac{d}{dt}\tilde{A}_{ij} + \tilde{A}_{ik}\tilde{A}_{kj} + \frac{2}{3}Q\delta_{ij} = 0. \tag{4}$$

The corresponding trace dynamics is given by equations

$$\frac{dQ}{dt} = -3R, \quad \frac{dR}{dt} = \frac{2}{3}Q^2, \tag{5}$$

in which $R\equiv-\tilde{A}_{ij}\tilde{A}_{jk}\tilde{A}_{ki}/3$ is the third invariant of tensor $\tilde{A}_{ij}$.

In RE dynamics, the discriminant of the characteristic polynomial of $\tilde{A}_{ij}$, $27R^2/4+Q^3\equiv Q_0^3$, is constant.[1,2] Therefore, when $Q_0\neq0$ the relevant variables in the above equations can be nondimensionalized by $t_*\equiv|Q_0|^{-1/2}$, giving

$$r = Rt_*^3, \quad q = Qt_*^2, \quad a_{ij} = t_*\tilde{A}_{ij}, \quad \tau = t/t_*. \tag{6}$$

When $Q_0=0$, one can replace Q_0 with the initial value of Q in the definition of t_*.[2] In terms of the nondimensionalized variables, Eqs. (4) and (5) will have the same forms, with the variables replaced by corresponding dimensionless ones. The discriminant becomes

$$27r^2/4 + q^3 = \mathrm{sgn}(Q_0). \tag{7}$$

Working with the nondimensionalized equations, Cantwell[2] showed that Eq. (4) admits an analytic solution. By taking the time derivative of the nondimensionalized version of Eq. (4), the following equation for a_{ij} has been obtained:[2]

$$\frac{d^2a_{ij}}{d\tau^2} + \frac{2}{3}q(\tau)a_{ij} = 0. \tag{8}$$

Further manipulations show that the solution to a_{ij} is a linear combination of two universal functions:

$$a_{ij}(\tau) = c_{ij}^0 f_1[r(\tau)] + d_{ij}^0 f_2[r(\tau)]. \tag{9}$$

The expressions of f_1 and f_2 will be given later when summarizing the key steps to obtain the solution for the material deformation tensor.

The evolution of deformation tensor $\mathbf{B}(\mathbf{X},t)$ evolves according to the following equation:[18]

$$\frac{dB_{ij}}{dt} = B_{ik}\tilde{A}_{kj}, \tag{10}$$

where $\tilde{A}_{ij}$ is the velocity gradient at the particle location. The equation suggests that the characteristic time scale of the evolution of B_{ij} is the same as that of $\tilde{A}_{ij}$. In the case of unfiltered velocity fields, it is expected to be proportional to the Kolmogorov time scale $\tau_K\equiv(\nu/\epsilon)^{1/2}$. For filtered velocity fields, it is expected to be proportional to the eddy turnover time scale at the filter scale, which is often taken as $[2\langle\tilde{S}_{ij}\tilde{S}_{ij}\rangle]^{-1/2}$, with $\tilde{S}_{ij}=(\tilde{A}_{ij}+\tilde{A}_{ji})/2$ being the filtered strain rate tensor.

In the context of RE dynamics, one can nondimensionalize the time scales for material deformation in the same way as before (taking into account that B_{ij} is already dimensionless), yielding

$$\frac{dB_{ij}}{d\tau} = B_{ik}a_{kj}. \tag{11}$$

Taking the time derivative of the above equation[2] and using Eq. (4), we find

$$\frac{d^2B_{ij}}{d\tau^2} = B_{il}a_{lk}a_{kj} + B_{ik}\left(-a_{kl}a_{lj} - \frac{2}{3}q\delta_{kj}\right) = -\frac{2}{3}q(\tau)B_{ij}. \tag{12}$$

Comparing with Eq. (8), it is apparent that in RE dynamics, B_{ij} obeys the same equation as a_{ij}. Therefore, the RE solu-

tion method[2] can also be applied to this equation. Specifically, a change of variables replacing τ with the time-like variable $s=(3\sqrt{3}/2)r(\tau)$ yields

$$[\mathrm{sgn}(Q_0)-s^2]\frac{d^2B_{ij}}{ds^2}-\frac{4}{3}s\frac{dB_{ij}}{ds}+\frac{2}{9}B_{ij}=0. \tag{13}$$

This equation can be solved[2] using hypergeometric functions by a further change of variables $x=1-s^2$ for $Q_0>0$ and $x=1+s^2$ for $Q_0<0$. Finally, the solution for B_{ij} can be written using the same general solutions as a_{ij}:

$$B_{ij}(\tau)=c_{ij}f_1(r)+d_{ij}f_2(r), \tag{14}$$

where the expressions for f_1 and f_2, having been obtained in Ref. 2, depend on the sign of the initial value of the discriminant. When $Q_0>0$:

$$f_1^+(r)=\frac{1}{2}\left[\left(1+\frac{3\sqrt{3}}{2}r\right)^{1/3}+\left(1-\frac{3\sqrt{3}}{2}r\right)^{1/3}\right], \tag{15}$$

$$f_2^+(r)=\frac{1}{\sqrt{3}}\left[\left(1+\frac{3\sqrt{3}}{2}r\right)^{1/3}-\left(1-\frac{3\sqrt{3}}{2}r\right)^{1/3}\right]. \tag{16}$$

When $Q_0<0$:

$$f_1^-(r)=\left(1+\frac{27}{4}r^2\right)^{1/6}\cos\left[\frac{1}{3}\tan^{-1}\left(\frac{3\sqrt{3}r}{2}\right)\right], \tag{17}$$

$$f_1^-(r)=\frac{2}{\sqrt{3}}\left(1+\frac{27}{4}r^2\right)^{1/6}\sin\left[\frac{1}{3}\tan^{-1}\left(\frac{3\sqrt{3}r}{2}\right)\right], \tag{18}$$

and when $Q_0=0$,

$$f_1^0(r)=2^{1/3}\left[\frac{3\sqrt{3}}{2}r\right]^{-2/3}, \tag{19}$$

$$f_2^0(r)=\frac{2^{2/3}}{3\sqrt{3}}\left[\frac{3\sqrt{3}}{2}r\right]^{2/3}. \tag{20}$$

The solutions depend on time through $r(\tau)$, whose analytic expressions have also been obtained[2] by solving the trace dynamics [Eq. (5)]. Eliminating $r(\tau)$ from the two equations, one obtains an equation for $q(\tau)$, whose solution can be written as an implicit function of τ. For the case when $Q_0>0$, the solution reads

$$F\left(\alpha,\sin\frac{5\pi}{12}\right)=\frac{2}{3^{1/4}}\tau, \tag{21}$$

with α related to $q(\tau)$ by the following equation:

$$\cos\alpha=\frac{1-\sqrt{3}-q(\tau)}{1+\sqrt{3}-q(\tau)}, \tag{22}$$

and where $F(\phi,k)$ is the incomplete elliptic function of the first kind with parameter k and amplitude ϕ, defined as

$$F(\phi,k)\equiv\int_0^{\phi}\frac{d\theta}{\sqrt{1-k^2\sin^2\theta}}. \tag{23}$$

The inverse of $F(\phi,k)$, giving the amplitude ϕ as a function of the value of F, is denoted as $\phi=\mathrm{am}(F)$. $\cos\phi$ is denoted as $\mathrm{cn}(F)$, and is called the "cosine amplitude" function. One then obtains

$$\cos\alpha=\mathrm{cn}[(2/3^{1/4})\tau]=\frac{1-\sqrt{3}-q(\tau)}{1+\sqrt{3}-q(\tau)}. \tag{24}$$

Thus, $q(\tau)$ can be explicitly written as

$$q^+(\tau)=\frac{(1-\sqrt{3})-(1+\sqrt{3})\mathrm{cn}\{[2/3^{1/4}]\tau\}}{1-\mathrm{cn}\{[2/3^{1/4}]\tau\}}. \tag{25}$$

With $q(\tau)$ given, $r(\tau)$ can then be obtained from Eq. (7). Similarly, the solutions for $Q_0<0$ and $Q_0=0$ can be found and are given in Ref. 2.

The coefficients c_{ij} and d_{ij} in the solution [Eq. (14)] are determined by the initial conditions for B_{ij}. By definition,

$$B_{ij}(0)=\delta_{ij}. \tag{26}$$

Thus, it follows from Eq. (11) that

$$dB_{ij}(0)/d\tau=a_{ij}(0). \tag{27}$$

Using these two initial conditions, c_{ij} and d_{ij} are found to be

$$c_{ij}=[q(\hat{r})]^2f_2'(\hat{r})\delta_{ij}-\tfrac{3}{2}f_2(\hat{r})\hat{a}_{ij}, \tag{28}$$

$$d_{ij}=\tfrac{3}{2}f_1(\hat{r})\hat{a}_{ij}-\hat{q}^2f_1'(\hat{r})\delta_{ij}, \tag{29}$$

where the prime denotes differentiation with respect to r and the hat denotes values of the quantities at $\tau=0$; i.e., $\hat{a}_{ij}\equiv a_{ij}(0)$, etc. We have assumed $r=\hat{r}$ when $\tau=0$. The solution as function of time can then be written as

$$B_{ij}(\tau)=g_1(r,\hat{r})\delta_{ij}+g_2(r,\hat{r})\hat{a}_{ij}. \tag{30}$$

where

$$g_1(r,\hat{r})=[q(\hat{r})]^2[f_2'(\hat{r})f_1(r)-f_1'(\hat{r})f_2(r)], \tag{31}$$

$$g_2(r,\hat{r})=\tfrac{3}{2}[f_1(\hat{r})f_2(r)-f_2(\hat{r})f_1(r)]. \tag{32}$$

The corresponding Cauchy-Green tensor can be written as follows:

$$C_{ij}(\tau)=g_1^2\delta_{ij}+g_1g_2(\hat{a}_{ij}+\hat{a}_{ji})+g_2^2\hat{a}_{ki}\hat{a}_{kj}. \tag{33}$$

Thus, we have obtained an analytic solution for the deformation and CG tensors, when the evolution of the velocity gradient tensor is approximated by restricted Euler dynamics. From the solution, the tensors **B** and **C** can be calculated after the velocity gradient is given at some initial time. Note that the solution depends on the initial velocity gradient not only through the coefficients in the solution, but also through the expressions of functions f_1 and f_2, which take different forms depending on the sign of the discriminant.

III. COMPARISON WITH DNS AND DISCUSSION

In this section, the analytic solutions to **B** and **C** are compared with DNS data of stationary isotropic turbulence. Analysis is conducted for both unfiltered and filtered fields. The turbulent velocity fields are generated by numerically solving the NS equation in a $[0,2\pi]^3$ box using a standard pseudospectral method. A statistically steady state is achieved by adding a forcing term to the NS equation that

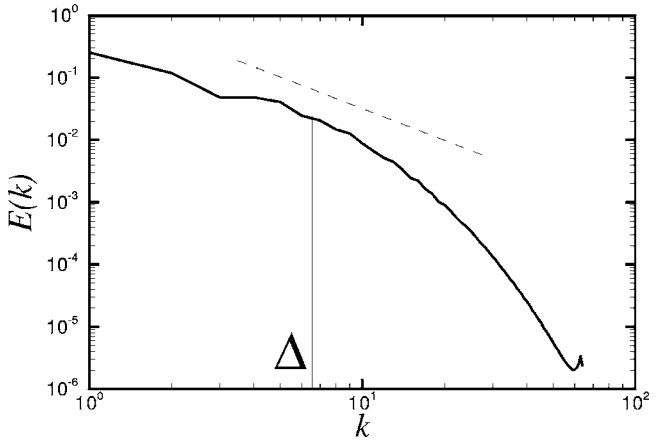

FIG. 2. Radial energy spectrum of the velocity field. Vertical line shows the filter scale.

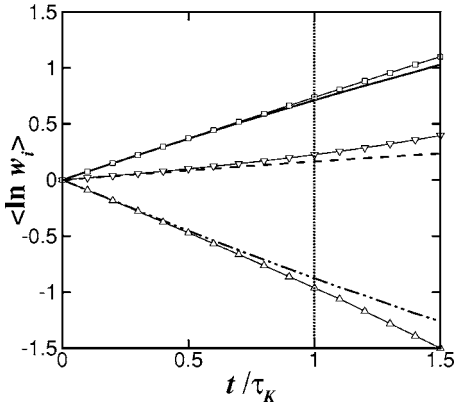

FIG. 4. Time evolution of the average value of the eigenvalues of the CG tensor. Thick lines: DNS; solid: $\ln w_1$; dashed: $\ln w_2$; dash-double-dotted: $\ln w_3$; thin solid line with symbols: RE; squares: $\ln w_1$; gradients: $\ln w_2$; deltas: $\ln w_3$.

feeds the turbulent field with kinetic energy at a constant rate. The grid resolution is 128^3, with Reynolds number $\mathrm{Re}_\lambda \approx 95$ and a Kolmogorov time scale $\tau_K \approx 0.17$. The size of time steps Δt of the simulation is calculated at each time step to keep the Courant number $\beta \equiv u_{\max}\Delta t/\Delta x \leq 0.15$, where $u_{\max}$ is the maximum velocity in the whole flow field at the time step and Δx is the grid width. Velocity fields separated in time by $\tau_K/10$ are stored for several τ_K after the steady state is reached, for subsequent analysis. As a reference, the energy spectrum of the steady state velocity field is shown in Fig. 2, where the vertical line marks the filter scale adopted in the ensuing analysis of filtered velocity fields.

1024^2 particles are followed in the velocity fields and the time series of B_{ij} are calculated both from DNS data and from the analytic solution Eq. (30). The former is obtained in a similar way as described in Ref. 18. Specifically, we numerically solve the equation of B_{ij} [Eq. (11)] along with the equation for particle locations

$$\frac{d\mathbf{x}}{dt} = \tilde{\mathbf{u}}(\mathbf{x},t), \tag{34}$$

where $\tilde{\mathbf{u}}$ is the velocity at the particle location. $\tilde{\mathbf{u}}$ is obtained from the stored velocity fields using a sixth-order Lagrangian interpolation. a_{ij} in Eq. (11) is obtained by the same scheme from the velocity gradient fields, which are calculated from the velocity fields in Fourier space and then transformed back to physical space. The numerical schemes for Eqs. (34) and (11) are taken from Ref. 18; i.e., we use a second-order Runge-Kutta scheme to calculate particle locations and a fourth-order one to calculate the deformation tensor. The integration time step used is the time step of the stored velocity data; i.e., $\tau_K/10$. Numerical tests have been performed with time step equal $\tau_K/34$ (see Ref. 18) to confirm that $\tau_K/10$ is small enough to obtain essentially step-size-independent results. For the RE part, we numerically solve the trace dynamics to obtain the time series of $q(t)$ and $r(t)$, starting from their DNS values for each particle. The numerical scheme is the same fourth-order Runge-Kutta scheme used to solve Eq. (11). Note that, although formally, the analytic solutions to

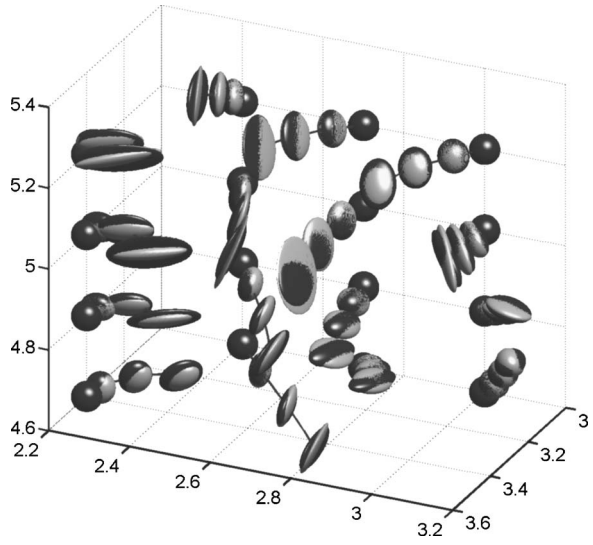

FIG. 3. Short time evolution of material elements from spheres into ellipsoids along several fluid particle trajectories. Ellipsoids defined by the corresponding CG tensor at $t=0.5\tau_K$, τ_K and $1.5\tau_K$ are shown, starting from spheres at $t=0$. Lines: the trajectories of the centers of the material elements, calculated from DNS data. Ellipsoids in dark color: DNS data; light color: analytic solution obtained with RE approximation.

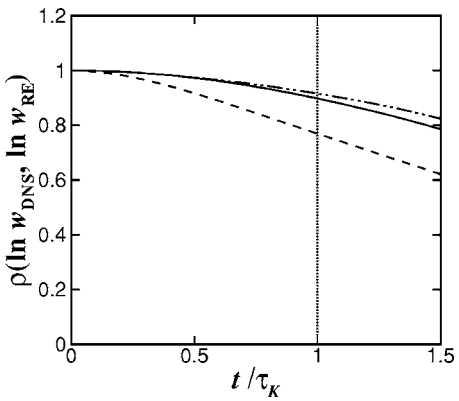

FIG. 5. Time evolution of the correlation coefficients between the eigenvalues of the CG tensor, calculated from DNS and RE. Solid line: $\ln w_1$; dashed: $\ln w_2$; dash-double-dotted: $\ln w_3$.

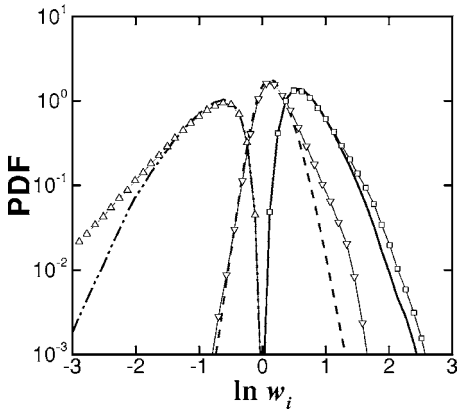

FIG. 6. Comparison of the PDFs of the logarithm of the eigenvalues, after evolution during one Kolmogorov time scale. Legend same as Fig. 4.

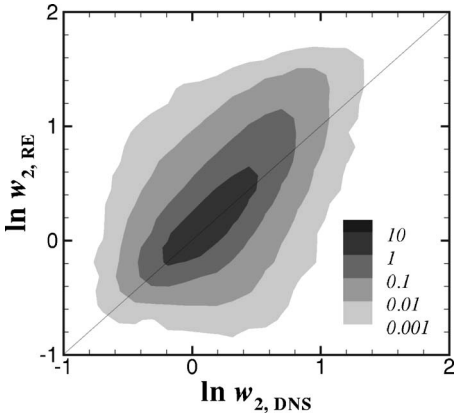

FIG. 8. Same as Fig. 7, but for $\ln w_2$.

$q(t)$ and $r(t)$ are available [see Eq. (25) and Ref. 2], they are in the form of (the inverse of) elliptical integrals. Therefore, we would have to resort to numerical integration anyhow to evaluate the solutions. Consequently, it is more straightforward to also integrate the differential equations for $q(t)$ and $r(t)$ numerically using the same scheme as for the deformation tensor elements. The coefficients c_{ij} and d_{ij} are also evaluated for each particle from the velocity gradient at its initial location. B_{ij} is then evaluated at each time t from the analytic solution using the known value of $r(t)$ and the coefficients.

Another point to note is that, due to the finite-time singularity inherent in RE dynamics, all initial conditions will inevitably tend to infinity at a certain time. In our procedure, the RE analytical predictions starting from the DNS initial conditions are recorded for up to two characteristic time scales (Kolmogorov or eddy turn-over time scale). During this time a small fraction of initial conditions will exhibit singular behavior. These must be excluded from the calculation of the statistics to be presented below. The procedure is as follows: For the comparison with unfiltered DNS data, a time series is excluded if any of the following three inequalities is violated: $\ln w_1 < 20$, $-10 < \ln w_2 < 10$, and $\ln w_3 > -20$. For the comparison with filtered DNS data, the inequalities are: $\ln w_1 < 40$, $-20 < \ln w_2 < 20$, and $\ln w_3 > -40$. The percentages of excluded time series are less than 1% in all cases.

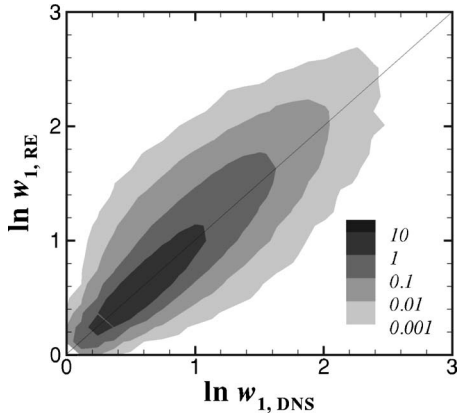

FIG. 7. Joint PDF of $\ln w_1$ calculated from DNS and RE after evolution during one Kolmogorov time scale.

The CG tensor **C** is calculated from the deformation tensor obtained in either way, and its eigenvalues and eigenvectors are evaluated. The eigenvalues w_i $(i=1,2,3)$ are ordered so that $w_1 \geq w_2 \geq w_3$. As mentioned before, an infinitesimal material element of a spherical shape deforms into an ellipsoid with the lengths of the axes given by the square roots of the eigenvalues of the associated CG tensor, and the direction of the axes given by corresponding eigenvectors. Therefore, before presenting quantitative comparisons, we visualize in Fig. 3 this process with several material elements. From Fig. 3 we can clearly see that significant deformation has occurred within $1.5\tau_K$. Almost all spheres are deformed into a pancake shape;[18] i.e., contracted in one direction and extended in the other two. Evolution of the shapes, defined by the lengths of the axes, and the orientations of the ellipsoids calculated from the RE solution follows the trend of DNS data closely, although there exist quantitative differences in both aspects, which increase as time progresses. In general it appears the ellipsoids calculated from the RE solution are flatter than those calculated from DNS data. We will quantify the difference in detailed comparisons that follows.

The results in unfiltered velocity fields are compared first. Shown in Fig. 4 is the time evolution of the average of the logarithm of the eigenvalues of **C**. The first item to note is that the evolution of the mean eigenvalues calculated from DNS data is in close agreement with the results of Ref. 18. Second, there is good agreement between the DNS and RE dynamics until about one Kolmogorov time scale, which is the characteristic time scale for the evolution of material deformation. As already noted, an infinitesimally small sphere evolves into an ellipsoid the lengths of whose axes are given by the square roots of w_i. By reading the figure, we can see that, at $t=\tau_K$, the ratio of the average longest to the average shortest axes of the ellipsoid is roughly

$$\frac{\ell_1}{\ell_3} \approx \left[\frac{e^{0.7}}{e^{-0.85}}\right]^{1/2} \approx 2.2. \tag{35}$$

Therefore, for average deformations, the RE dynamics agrees quite well with DNS even when significant average

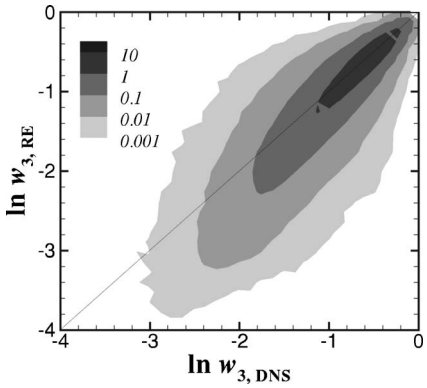

FIG. 9. Same as Fig. 7, but for $\ln w_3$.

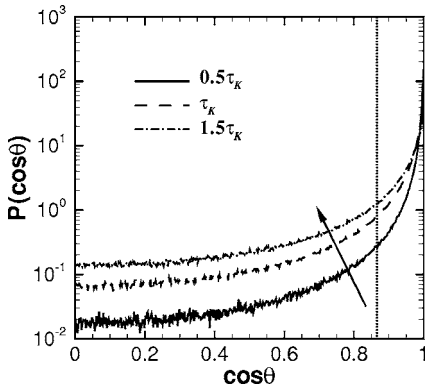

FIG. 11. Same as Fig. 10, but for the eigenvector corresponding to the intermediate eigenvalue.

deformation has occurred. Figure 5 shows the correlation coefficients between the eigenvalues calculated from DNS and from RE dynamics. The correlation for both the most extensive and contractive eigenvalues are more than 90% at $t=\tau_K$. It is interesting to note that the correlation is smaller between the intermediate ones, slightly below 80% at $t=\tau_K$.

The probability density functions (PDFs) of the logarithmic eigenvalues measured at τ_K are compared in Fig. 6. The agreement is good around the peaks as well as near the low-magnitude regions of the PDFs. The left tail of the PDF of the contractive eigenvalue w_3 from RE dynamics is significantly above that calculated from DNS data, which means the fluid elements are more contracted in RE dynamics. This is a signature of the RE dynamics approaching finite time singularity[2] for some fluid particles, which confirms that the singularity is a consequence of excessive squeezing of fluid elements. This unrealistically strong contraction is accompanied by the excessive extension in both the most extensive and the intermediate eigen-directions, as is shown by the higher right tails of the PDFs of the two corresponding eigenvalues. It is interesting to see that excessive extension in the intermediate direction is more probable than in the most extensive direction. The difference between the PDFs calculated from RE dynamics and DNS data seems to suggest that the pancake shape taken by the fluid elements in RE dynamics is more likely to be flatter, of smaller thickness, and rounder in its shape. This appears to be supported by the visualization in Fig. 3. According to the PDF of $\ln w_2$ in Fig. 6, and as already found in Ref. 18, $\ln w_2$ is more probable to take positive values. This means that it is more probable to observe a sphere to be deformed to a pancake shape than to a cigar shape. The joint PDFs of the logarithmic eigenvalues of **C** calculated from RE and DNS shown in Figs. 7–9 clearly identify strong correlations between the eigenvalues calculated from RE dynamics and DNS, consolidating the results in Fig. 5. In addition, in Fig. 7, the lower-value contours of the joint PDF between $\ln w_1$ are biased toward the upper half of the coordinate plane, consistent with the higher right tail of the PDF of $\ln w_1$ calculated from RE dynamics plotted in Fig. 6. The consistency is also seen in the plots of the other two eigenvalues.

Next, the relative orientations of the eigenvectors calculated from RE dynamics and DNS are compared. The PDFs of $\cos\theta \equiv |\mathbf{e}_i^{\mathrm{RE}} \cdot \mathbf{e}_i^{\mathrm{DNS}}|$ are plotted (no summation is implied), where $\mathbf{e}_i$ is the ith eigenvector, and thus θ is the angle between the eigenvectors calculated from DNS data and the analytic solution to the RE approximation. Figures 10–12 are the results for the eigenvectors corresponding to the most extensive, intermediate and contractive directions, respectively. PDFs at three times are shown. Note that if there were no preferential alignments the PDFs would take a constant value of 1. In general the alignment deteriorates as time

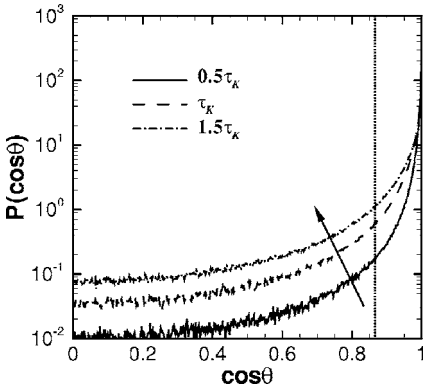

FIG. 10. The PDF of the angle between the eigenvectors of the Cauchy-Green tensor calculated from DNS and RE: the eigenvector corresponding to the most extensive eigenvalue.

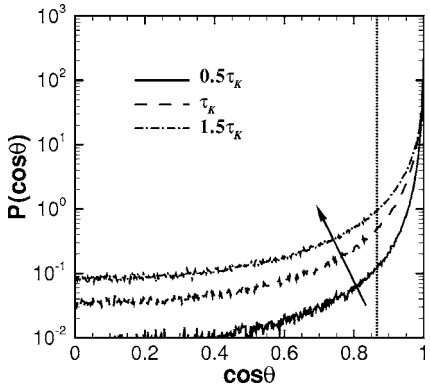

FIG. 12. Same as Fig. 10, but for the eigenvector corresponding to the contractive eigenvalue.

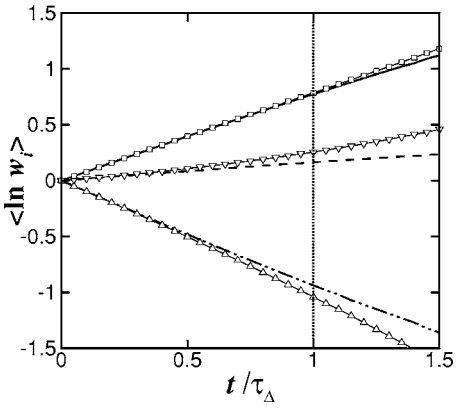

FIG. 13. Same as Fig. 4, but for filtered DNS data.

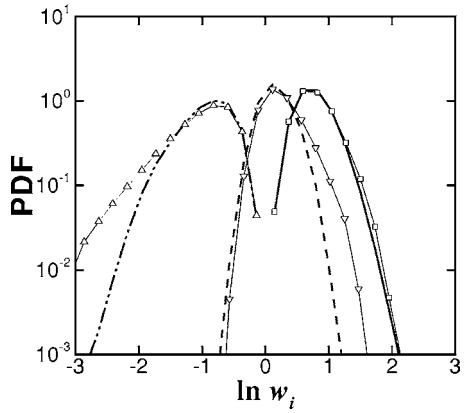

FIG. 15. Comparison of the PDFs of the logarithm of the eigenvalues at one eddy turn-over time scale at the filter scale. Legend same as Fig. 4.

progresses. However, good alignment is still obtained at τ_K. The area under each curve to the right of the vertical dashed lines gives the percentage of data that has alignment such that $\cos\theta > \cos 30° \approx 0.866$, or equivalently, alignment better than 30°. At τ_K, the percentage is 92% for the most extensive eigen-direction, 86% for the intermediate one, and 93% for the contractive one. Note that to completely determine the orientation of the three axes of one coordinate system relative to those of another, one needs to use a joint PDF of three suitably defined angles (see, for example, Ref. 25 for an intuitive definition of the angles). We have also measured such a joint PDF (not shown), only to confirm that the most probable alignment always occurs at $\theta=0$ for all eigen-directions. Comparisons among Figs. 10–12 seem to suggest that the alignment between the eigenvectors corresponding to the contractive direction is better than the other two.

The same analysis is repeated for the DNS data filtered at a length scale $\Delta=20\eta$, where $\eta\equiv(\nu^3/\epsilon)^{1/4}$ is the Kolmogorov length scale. The local turn-over time scale τ_Δ is defined according to $\tau_\Delta=\alpha(2\langle\tilde{S}_{ij}\tilde{S}_{ij}\rangle)^{-1/2}$, where $\alpha=1.0$. The value of α is chosen to ensure that, when $\Delta=\eta$, the time scale calculated from this definition has the same value as the value of τ_K. With this definition, $\tau_\Delta\approx 0.34$ in our filtered DNS data. Notice that since the anisotropic SGS stress has been neglected in the RE dynamics, the analytic solutions for either the velocity gradient or the deformation tensor in filtered velocity fields remain the same. The difference between the behaviors of the velocity gradient or the deformation tensor in filtered velocity fields is solely due to the difference in the initial value of the velocity gradient. Figures 13–15 show, respectively, the time evolution of the mean of the eigenvalues, the correlation coefficients between the prediction of RE solution and DNS, and the PDFs of eigenvalues at $t=\tau_\Delta$. Generally speaking, the same trends as for the unfiltered DNS data are observed. One difference is that the agreement between RE solution and filtered DNS data decreases slightly faster than in the previous case. On the other hand, Figs. 13 and 15 show that the agreement in $\ln w_1$, the largest eigenvalue, is better compared with the case for unfiltered velocity fields. Results concerning the alignment between eigenvectors (not shown) also display similar trends as for unfiltered velocity fields.

Finally, we make a comparison in Fig. 16 between the mean rates of increase of the logarithmic eigenvalues (the Lyapunov exponents) obtained from the filtered and unfiltered DNS data. It is shown in Fig. 16 that, for the unfiltered data, the mean rates of increase of the logarithmic eigenvalues approach constant values after about ten Kolmogorov time scales. The results are 0.3 for $\ln w_1$, 0.05 for $\ln w_2$ and

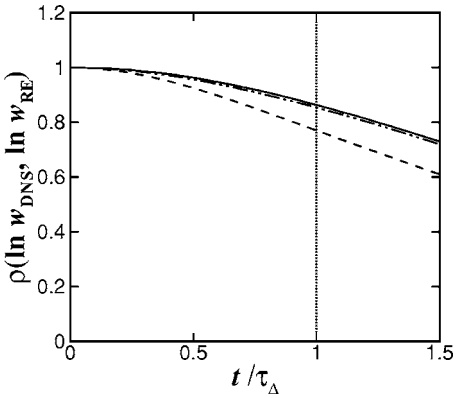

FIG. 14. Same as Fig. 5, but for filtered DNS data.

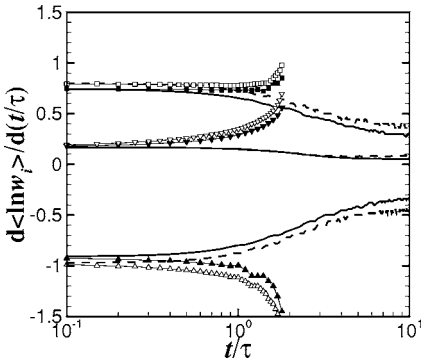

FIG. 16. The rates of increase of the logarithmic eigenvalues. Solid lines: unfiltered DNS data; dashed lines: filtered DNS data with filter scale $\Delta=20\eta$. Solid symbols: RE solutions using unfiltered DNS data as initial conditions; empty symbols: RE solutions with filtered DNS data as initial conditions. The top group of curves is the results for $\ln w_1$, middle $\ln w_2$, and bottom $\ln w_3$. The time scale τ equals τ_K for unfiltered DNS results and τ_Δ for filtered.

−0.35 for $\ln w_3$, nearly the same as the values found in Ref. 18. For filtered DNS data, the time evolution of the results follows the same trends as that of unfiltered data, but the magnitude is slightly larger. At about ten eddy turn-over times ($10\tau_\Delta$), the rates of increase also approach constant values of 0.35, 0.1, and −0.45 for $\ln w_1$, $\ln w_2$, and $\ln w_3$, respectively. These values show that the average stretching efficiency of material elements is quite similar between filtered turbulence in the inertial range and unfiltered velocity fields at the viscous scale. However, we must point out that the curves for filtered DNS data plotted in Fig. 16 depend on the value of α in our definition of τ_Δ. When α is smaller, one obtains smaller asymptotic values. The results calculated from the RE analytic solution are also plotted in Fig. 16, showing again that the agreement is good up to about one characteristic time scale.

IV. CONCLUSIONS

In this paper the evolution of material deformation in restricted Euler dynamics is investigated. It is shown that when the evolution of the velocity gradient tensor is approximated by restricted Euler dynamics, the equation of the deformation tensor allows for an analytic solution. The solution can be expressed as linear combination of universal functions.[2] The evolution of material deformation predicted from the analytic solution is compared with filtered and unfiltered DNS data. Within the time scale that characterizes the evolution of material deformation, good agreement is obtained both in terms of the eigenvalues of the Cauchy-Green tensor and the alignment of the corresponding eigenvectors. The analytic solution thus provides a compact parameterization of the short time behavior of material deformation, which is conceivably useful in certain circumstances. The discrepancy between the restricted Euler solution and DNS data results from the neglected terms in the restricted Euler equation for the velocity gradient. To understand the effects of the neglected terms on the evolution of material deformation is another interesting question that requires further investigation.

ACKNOWLEDGMENTS

We thank Dr. Laurent Chevillard for useful discussions. We gratefully acknowledge the support of the National Science Foundation (ITR-0428325).

[1] P. Vieillefosse, "Local interaction between vorticity and shear in a perfect incompressible fluid," J. Phys. (France) **43**, 837 (1982).
[2] B. J. Cantwell, "Exact solution of a restricted Euler equation for the velocity gradient tensor," Phys. Fluids A **4**, 782 (1992).
[3] J. Martin, A. Ooi, M. S. Chong, and J. Soria, "Dynamics of the velocity gradient tensor invariants in isotropic turbulence," Phys. Fluids **10**, 2336 (1998).
[4] K. K. Nomura and G. K. Post, "The structure and dynamics of vorticity and rate of strain in incompressible homogeneous turbulence," J. Fluid Mech. **377**, 65 (1998).
[5] A. Ooi, J. Martin, J. Soria, and M. S. Chong, "A study of evolution and characteristics of the invariants of the velocity-gradient tensor in isotropic turbulence," J. Fluid Mech. **381**, 141 (1999).
[6] B. Lüthi, A. Tsinober, and W. Kinzelbach, "Lagrangian measurement of vorticity dynamics in turbulent flow," J. Fluid Mech. **528**, 87 (2005).
[7] M. Guala, B. Lüthi, A. Liberzon, A. Tsinober, and W. Kinzelbach, "On the evolution of material lines and vorticity in homogeneous turbulence," J. Fluid Mech. **533**, 339 (2005).
[8] F. van der Bos, B. Tao, C. Meneveau, and J. Katz, "Effects of small-scale turbulent motions on the filtered velocity gradient tensor as deduced from holographic particle image velocimetry measurements," Phys. Fluids **14**, 2456 (2002).
[9] W. T. Ashurst, A. R. Kerstein, R. M. Kerr, and C. H. Gibson, "Alignment of vorticity and scalar gradient with strain rate in simulated Navier-Stokes turbulence," Phys. Fluids **30**, 2343 (1987).
[10] A. Tsinober, E. Kit, and T. Dracos, "Experimental investigation of the field of velocity-gradients in turbulent flows," J. Fluid Mech. **242**, 169 (1992).
[11] T. S. Lund and M. M. Rogers, "An improved measure of strain state probability in turbulent flows," Phys. Fluids **6**, 1838 (1994).
[12] S. S. Girimaji and S. B. Pope, "A diffusion model for velocity gradients in turbulence," Phys. Fluids A **2**, 242 (1990).
[13] M. Chertkov, A. Pumir, and B. I. Shraiman, "Lagrangian tetrad dynamics and the phenomenology of turbulence," Phys. Fluids **11**, 2394 (1999).
[14] E. Jeong and S. S. Girimaji, "Velocity-gradient dynamics in turbulence: Effect of viscosity and forcing," Theor. Comput. Fluid Dyn. **16**, 421 (2003).
[15] A. Naso and A. Pumir, "Scale dependence of the coarse-grained velocity derivative tensor structure in turbulence," Phys. Rev. E **72**, 056318 (2005).
[16] L. Chevillard and C. Meneveau, "Lagrangian dynamics and statistical geometric structure of turbulence," Phys. Rev. Lett. **97**, 174501 (2006).
[17] R. W. Ogden, *Non-linear Elastic Deformations* (Ellis Horwood, West Sussex, UK, 1984).
[18] S. S. Girimaji and S. B. Pope, "Material element deformation in isotropic turbulence," J. Fluid Mech. **220**, 427 (1990).
[19] W. J. Cocke, "Turbulent hydrodynamic line stretching: Consequences of isotropy," Phys. Fluids **12**, 2488 (1969).
[20] S. A. Orszag, "Comments on 'Turbulent hydrodynamic line stretching: Consequences of isotropy'," Phys. Fluids **13**, 2203 (1970).
[21] G. K. Batchelor, "The effects of homogeneous turbulence on material lines and surfaces," Proc. R. Soc. London, Ser. A **213**, 349 (1952).
[22] J. Duplat and E. Villermaux, "Persistency of material element deformation in isotropic flows and growth rate of lines and surfaces," Eur. Phys. J. B **18**, 353 (2000).
[23] S. Kida and S. Goto, "Line statistics: Stretching rate of passive lines in turbulence," Phys. Fluids **14**, 352 (2002).
[24] V. Borue and S. A. Orszag, "Local energy flux and subgrid-scale statistics in three-dimensional turbulence," J. Fluid Mech. **366**, 1 (1998).
[25] B. Tao, J. Katz, and C. Meneveau, "Statistical geometry of subgrid-scale stresses determined from holographic particle image velocimetry measurements," J. Fluid Mech. **457**, 35 (2002).